Supplementary Information

Harnessing chloride to drive catalyst reconstruction for durable and efficient seawater electrolysis

Huangcong Tang,[1] Zemin Feng,[1] Di Feng,[1] Shunchun Yao,[2] Kui Shen,[1] Liyu Chen,[1,*] Yingwei Li[1,*]

[1] Guangdong Provincial Key Laboratory of Fuel Cell Technology, School of Chemistry and Chemical Engineering, South China University of Technology, Guangzhou 510640, China.

[2] School of Electric Power Engineering, South China University of Technology, 510640, Guangzhou, China.

*Corresponding authors. Email: liyuchen@scut.edu.cn; liyw@scut.edu.cn

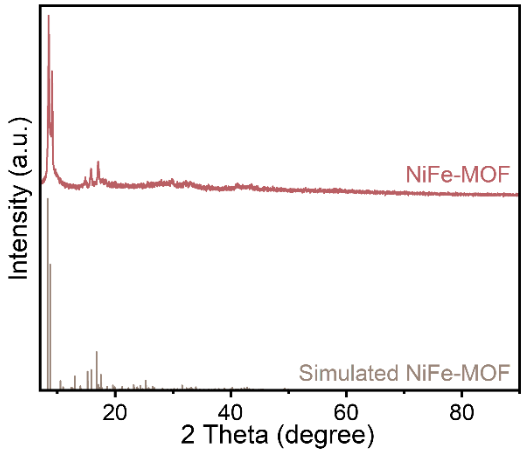

Fig. S1. XRD patterns of NiFe-MOF detached from the NF substrate.

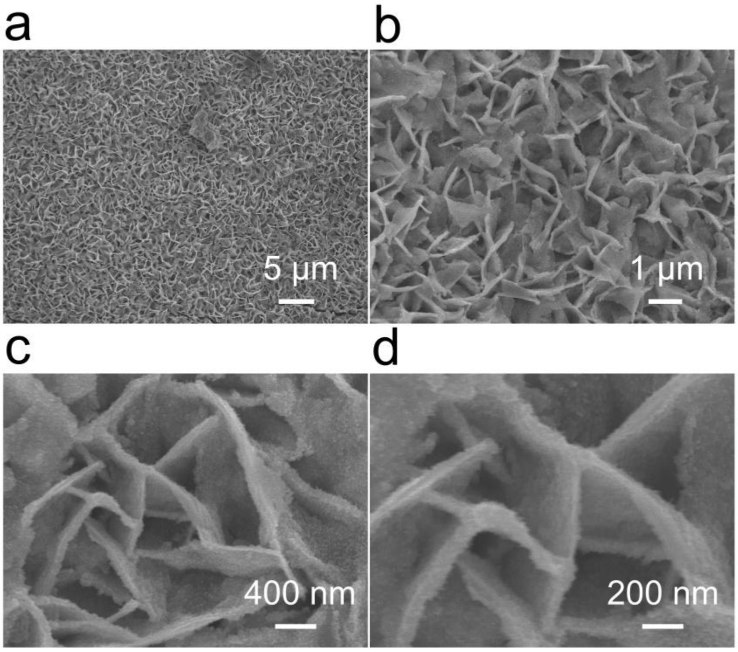

Fig. S2. SEM images of NiFe-MOF/NF.

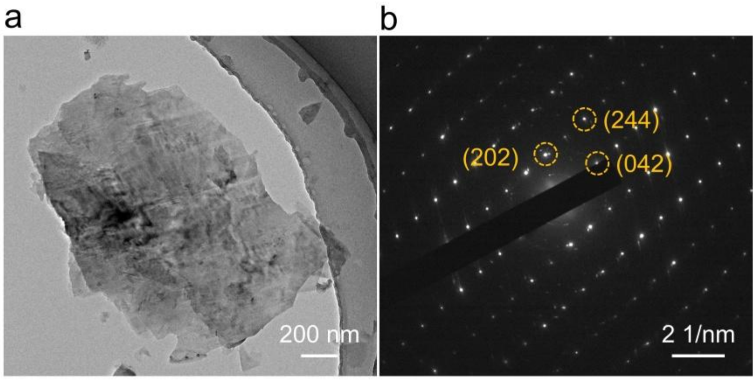

Fig. S3. (a) TEM image and (b) SAED patterns of NiFe-MOF detached from the NF substrate.

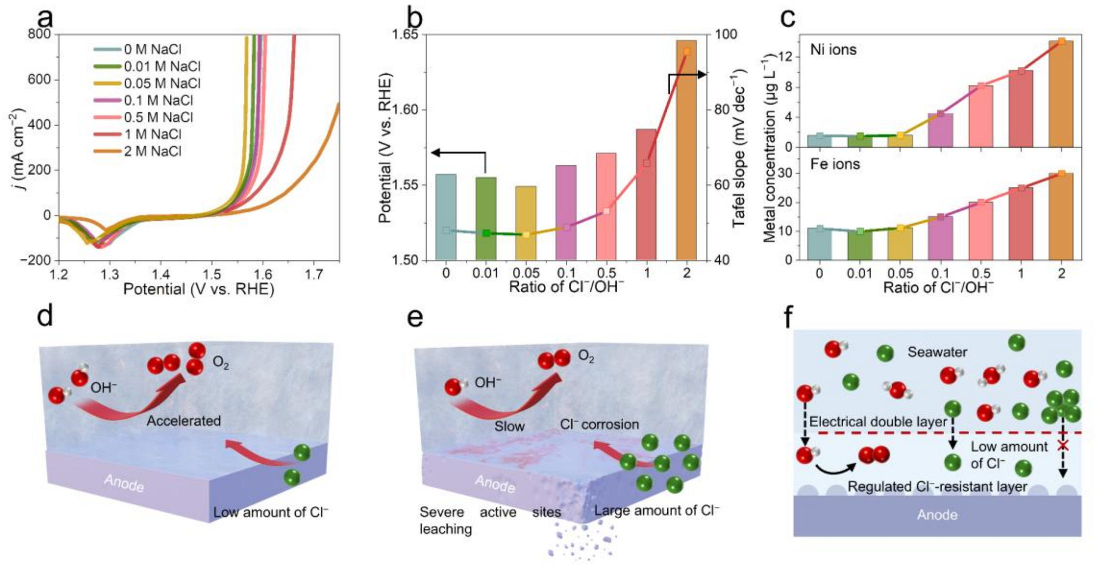

Fig. S4. Effect of Cl^- concentration on OER performance. (a) The LSV polarization curves for NiFe-MOF/NF in electrolytes with different Cl^-/OH^- ratios in 1 M KOH. (b) Comparison of potentials at a current density of 100 mA cm^{-2} and Tafel slopes. (c) The dissolution concentrations of Ni ions and Fe ions during CP tests for 24 hours in different electrolytes. (d, e) The schematic diagram of Cl^- effect with (d) low and (e) large amount of Cl^-/OH^- ratios in 1 M KOH. (f) The proposed strategy to utilize traces of Cl^- to promote OER performance in seawater electrolysis.

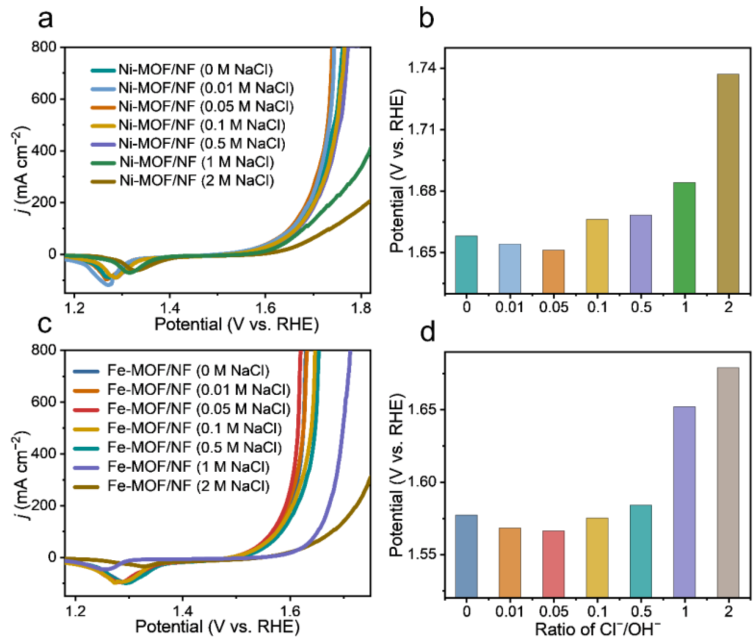

Fig. S5. (a, c) The LSV polarization curves for (a) Ni-MOF/NF and (c) Fe-MOF/NF in electrolytes with different Cl^-/OH^- ratios in 1 M KOH. (b, d) Comparison of potentials for (b) Ni-MOF/NF and (d) Fe-MOF/NF at a current density of 100 mA cm^{-2}.

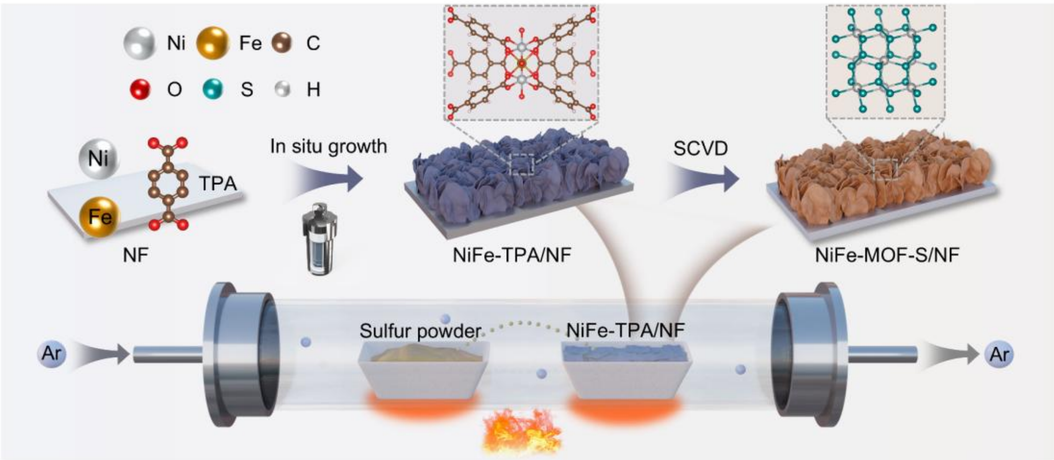

Fig. S6. Schematic illustration of the synthetic process of NiFe-MOF-S/NF.

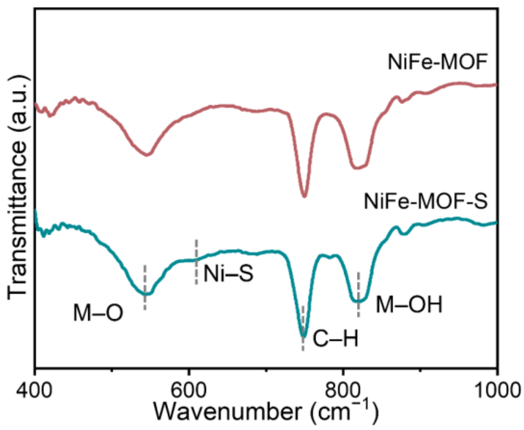

Fig. S7. FTIR spectra of NiFe-MOF and NiFe-MOF-S detached from the NF substrate.

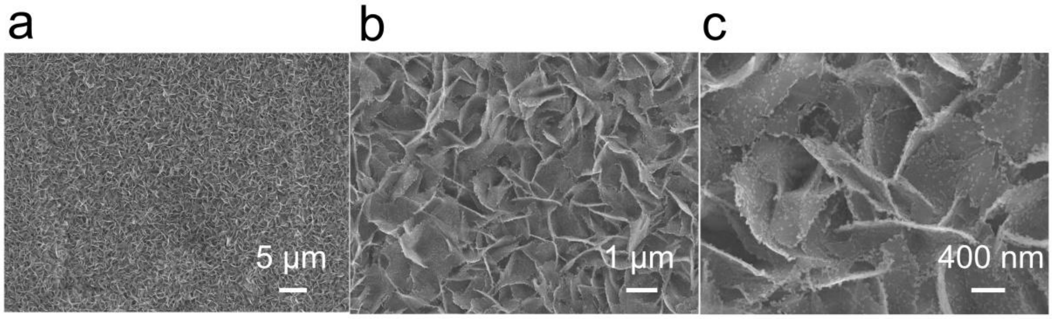

Fig. S8. SEM images of NiFe-MOF-S/NF.

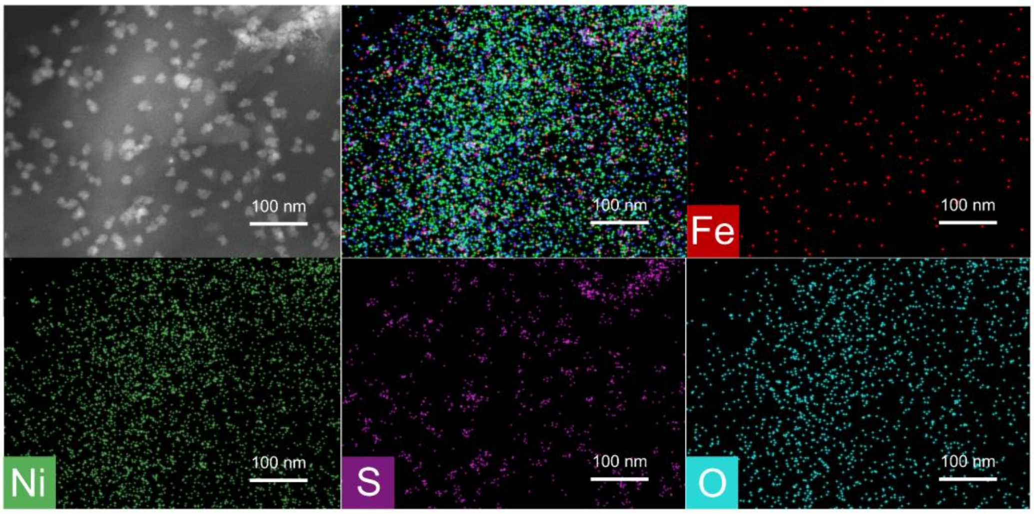

Fig. S9. HAADF-STEM image and the elemental mappings of NiFe-MOF-S detached from the NF substrate.

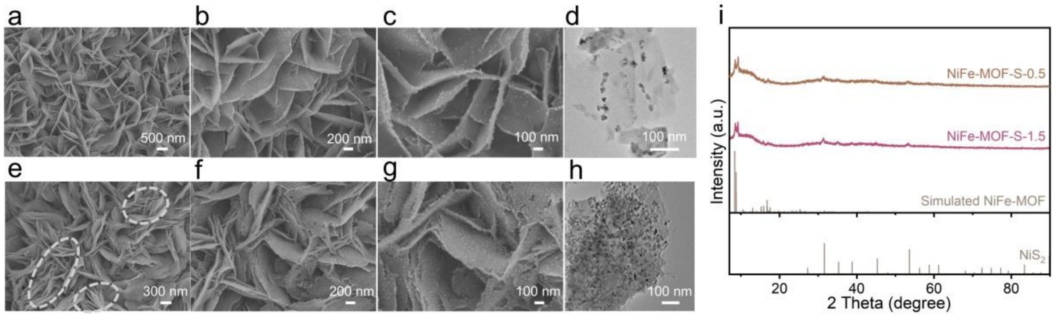

Fig. S10. SEM images of (a–c) NiFe-MOF-S-0.5/NF, (e–g) NiFe-MOF-S-1.5/NF. (d, h) TEM images of (d) NiFe-MOF-S-0.5 and (h) NiFe-MOF-S-1.5 detached from the NF substrate. (i) XRD patterns of NiFe-MOF-S-0.5 and NiFe-MOF-S-1.5 (NiS_2: PDF#11-0099).

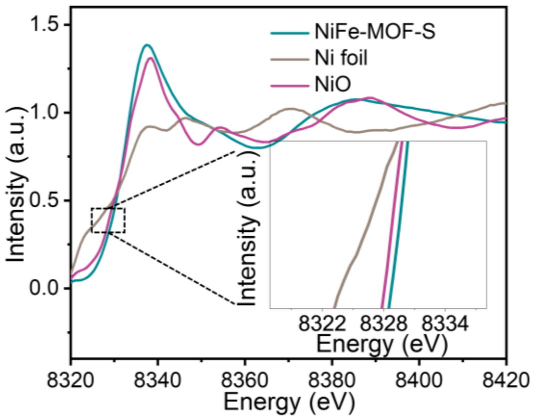

Fig. S11. Ni K-edge XANES spectra of Ni foil, NiO, and NiFe-MOF-S detached from the NF substrate (inset: expanded view of the absorption edge region).

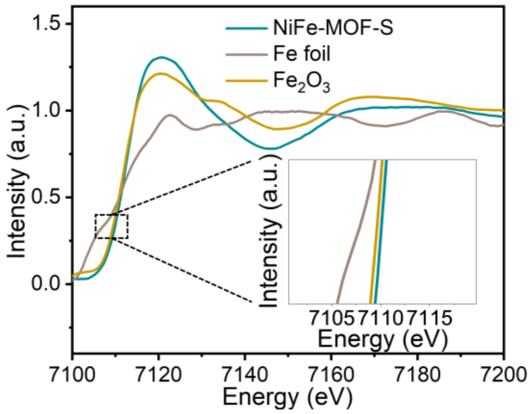

Fig. S12. Fe K-edge XANES spectra of Fe foil, Fe_2O_3, and NiFe-MOF-S detached from the NF substrate (inset: expanded view of the absorption edge region).

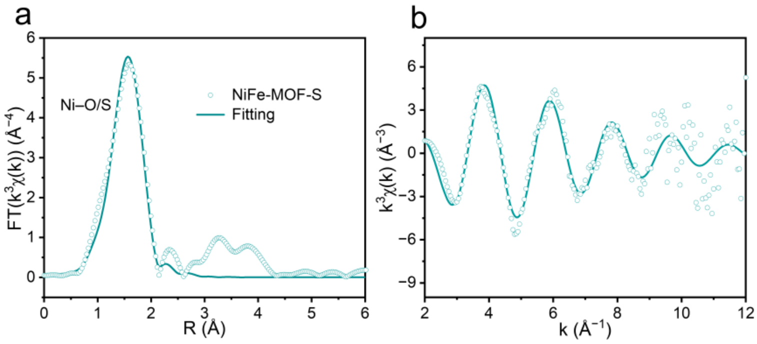

Fig. S13. The fitting analysis of k^3-weighted Fe K-edge EXAFS oscillations of NiFe-MOF-S detached from the NF substrate in k space (b) and FT to R space (a) (R represents the radial distance, and k is the wavelength of the oscillation).

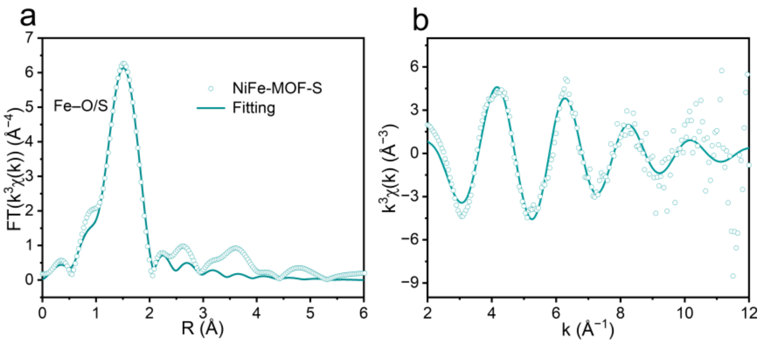

Fig. S14. The fitting analysis of k^3-weighted Fe K-edge EXAFS oscillations of NiFe-MOF-S detached from the NF substrate in (b) k space and (a) FT to R space.

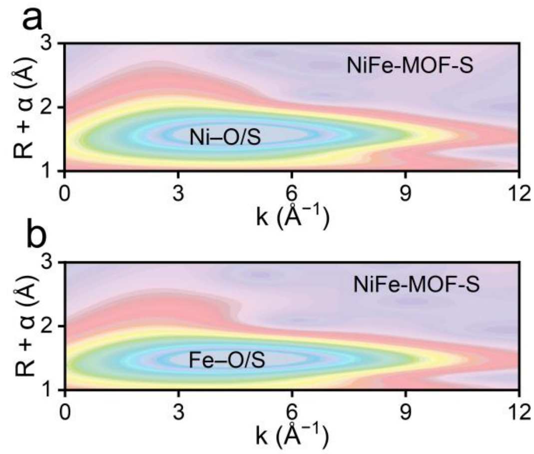

Fig. S15. The WT k^3-weighted EXAFS plots of (a) Ni and (b) Fe for NiFe-MOF-S detached from the NF substrate.

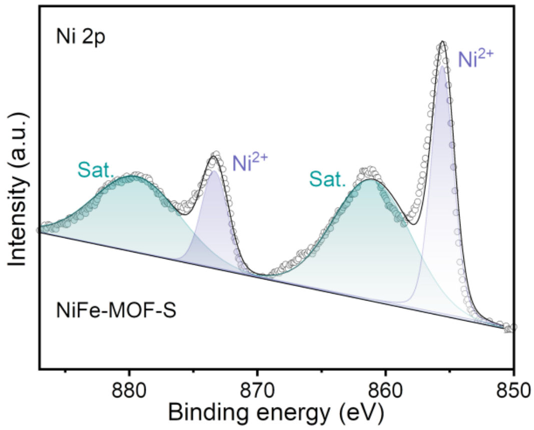

Fig. S16. XPS spectrum of Ni 2p for NiFe-MOF-S detached from the NF substrate.

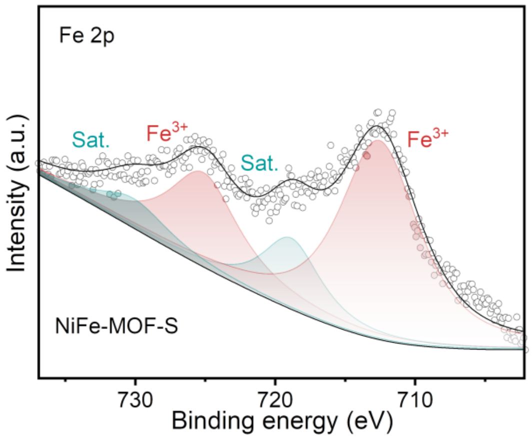

Fig. S17. XPS spectrum of Fe 2p for NiFe-MOF-S detached from the NF substrate.

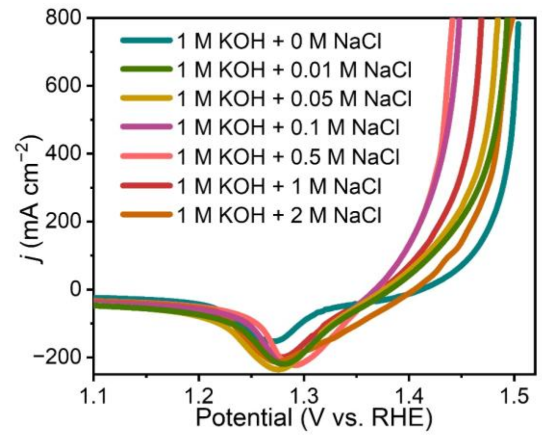

Fig. S18. The LSV polarization curves for NiFe-MOF-S/NF in electrolytes with different Cl^-/OH^- ratios in 1 M KOH.

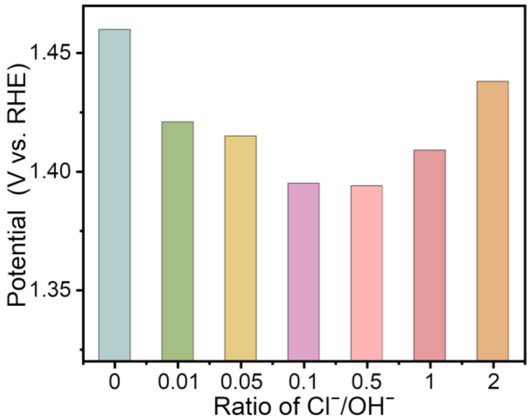

Fig. S19. Comparison of OER potential at a current density of 100 mA cm^{-2} for NiFe-MOF-S/NF in electrolyte with different Cl^-/OH^- ratios in 1 M KOH.

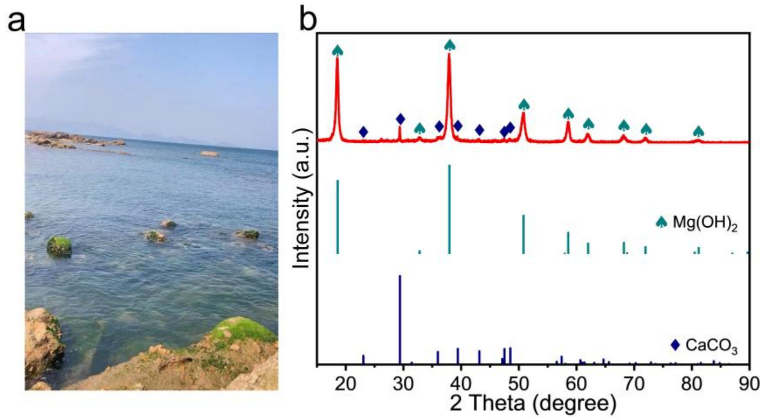

Fig. S20. (a) Photograph of the location of seawater sampling on 25/7/2023. The raw seawater was collected from Nantun Wharf in Qingdao, Shandong province, China–34.16 N, 122.67 E. (b) XRD pattern of white precipitations ($CaCO_3$: PDF#86-2334; $Mg(OH)_2$: PDF#82-2453).

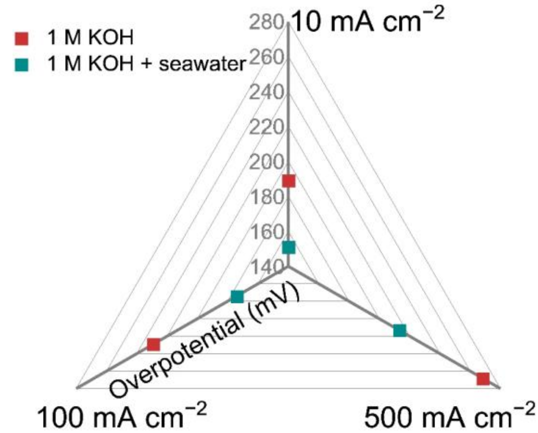

Fig. S21. The overpotentials of NiFe-MOF-S/NF to achieve 10, 100, and 500 mA cm^{-2} in 1 M KOH and 1 M KOH + seawater.

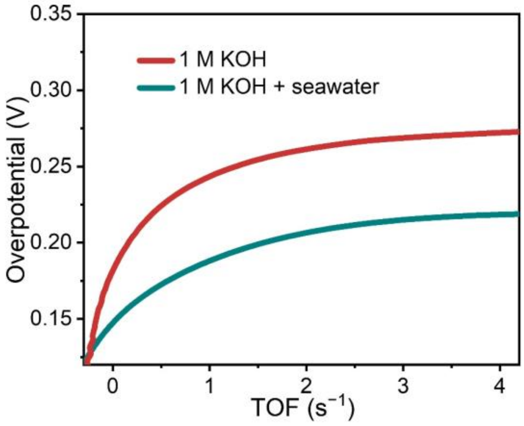

Fig. S22. TOF of NiFe-MOF-S/NF at different overpotentials in 1 M KOH and 1 M KOH + seawater.

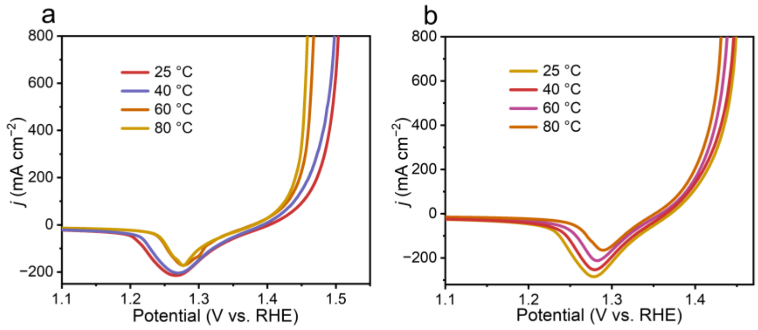

Fig. S23. LSV polarization curves as a function of temperatures for NiFe-MOF-S/NF in (a) 1 M KOH and (b) 1 M KOH + seawater.

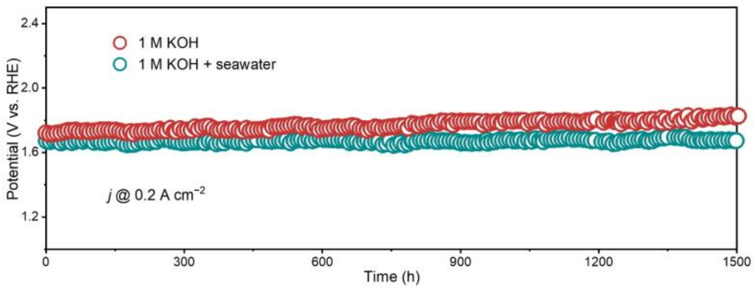

Fig. S24. OER durability test at a current density of 0.2 A cm^{-2} for NiFe-MOF-S/NF in 1 M KOH and 1 M KOH + seawater.

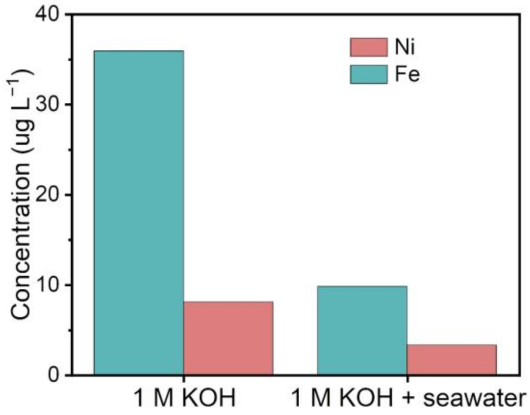

Fig. S25. The Ni and Fe concentrations in the electrolyte during OER for NiFe-MOF-S/NF in 1 M KOH and 1 M KOH + seawater.

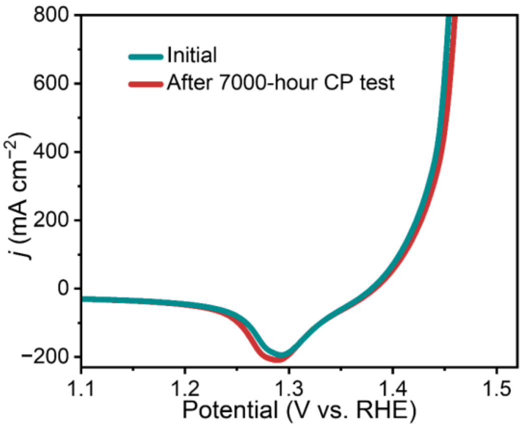

Fig. S26. LSV polarization curves of NiFe-MOF-S/NF before and after 7000-hour CP test in 1 M KOH + seawater.

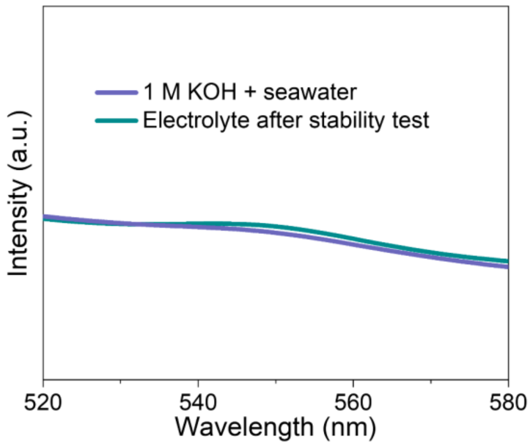

Fig. S27. UV-vis absorption spectra of electrolyte after stability tests with N,N-diethyl-p-phenylenediamine.

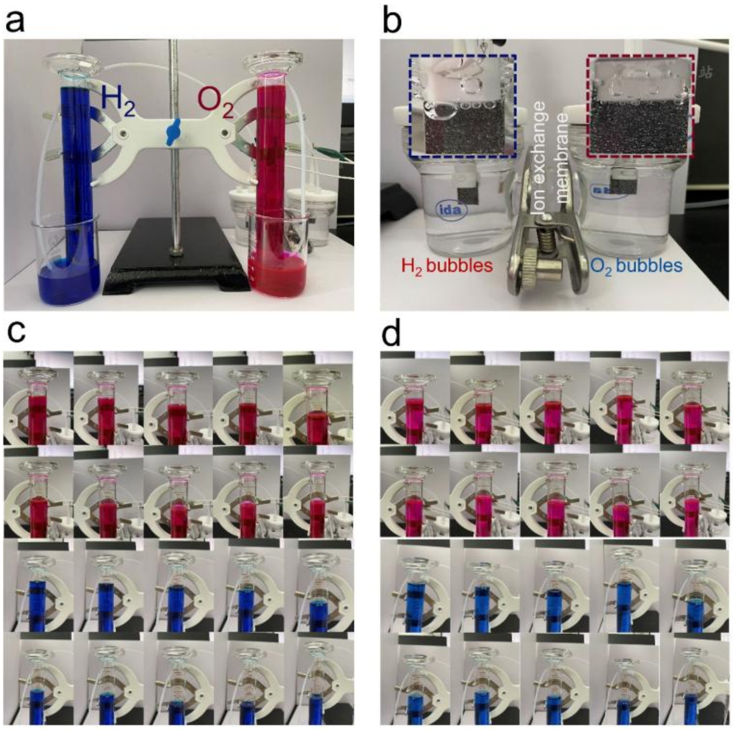

Fig. S28. (a, b) Home-made gas measuring device, the gas amount of H_2 and O_2 in (c) 1 M KOH and (d) 1 M KOH + seawater of NiFe-MOF-S/NF.

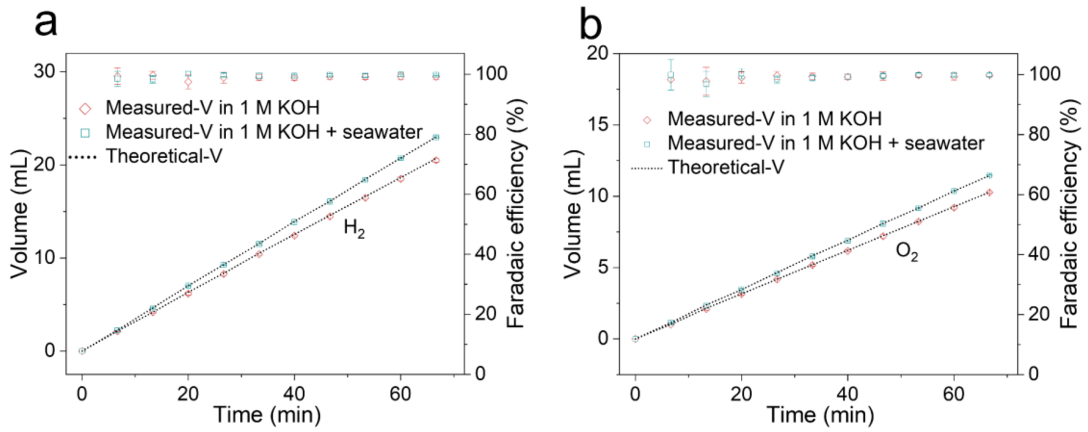

Fig. S29. The produced (a) H_2 and (b) O_2 quantity during overall splitting of NiFe-MOF-S/NF in 1 M KOH and 1 M KOH + seawater.

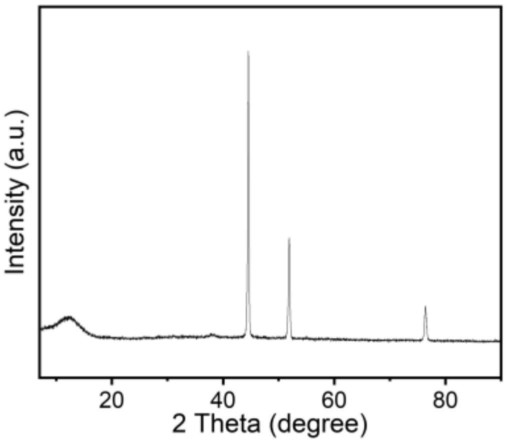

Fig. S30. XRD patterns of NiFe-MOF-S/NF after 7000-hour durability test in 1 M KOH + seawater.

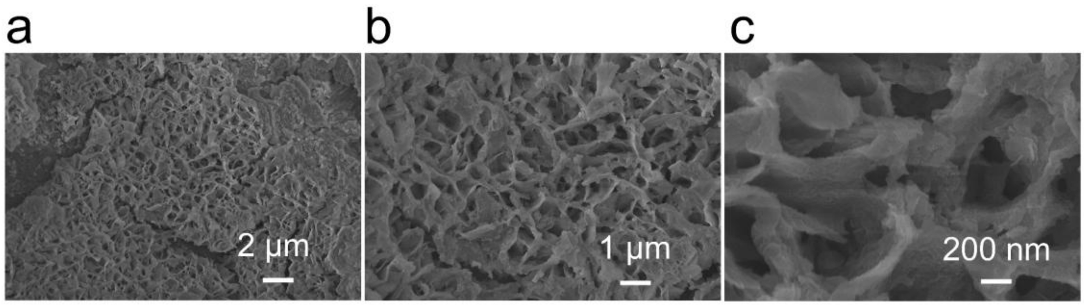

Fig. S31. SEM images of NiFe-MOF-S/NF after 7000-hour durability test in 1 M KOH + seawater.

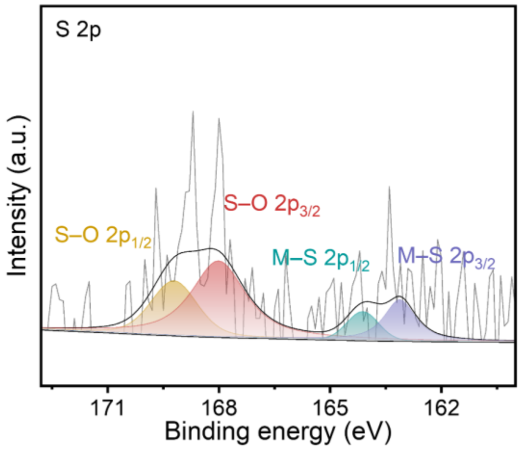

Fig. S32. XPS spectrum of S 2p for NiFe-MOF-S after 7000-h durability test at 1.0 A cm^{-2} in 1 M KOH + seawater.

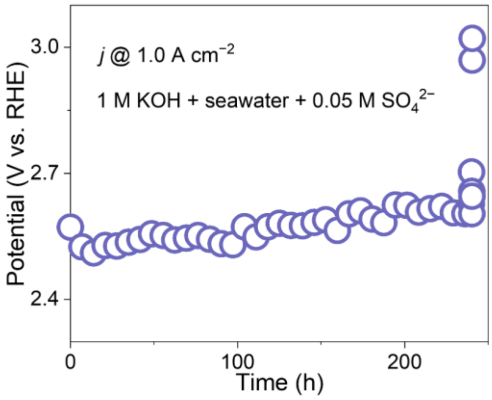

Fig. S33. OER durability test at 1.0 A cm^{-2} for NiFe-MOF/NF in 1 M KOH + seawater with 0.05 M Na_2SO_4.

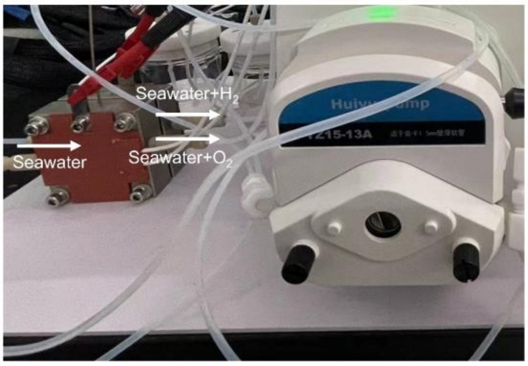

Fig. S34. The optical photos of AEMWE electrolyzer.

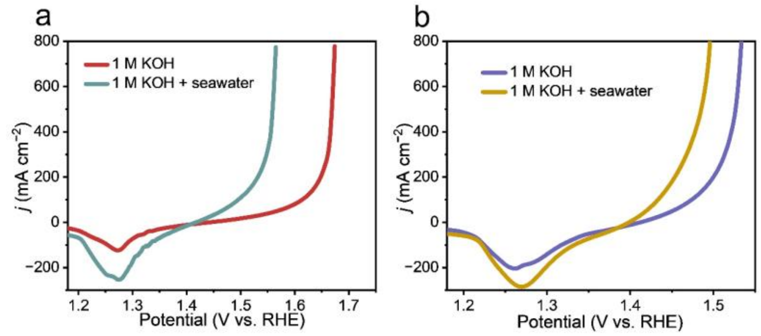

Fig. S35. LSV polarization curves of (a) Ni-MOF-S/NF and (b) Fe-MOF-S/NF in 1 M KOH and 1 M KOH + seawater.

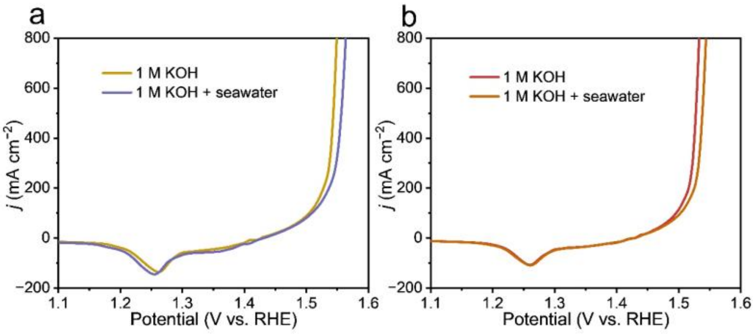

Fig. S36. LSV polarization curves of (a) NiFe-MOF-S-0.5/NF and (b) NiFe-MOF-S-1.5/NF in 1 M KOH and 1 M KOH + seawater.

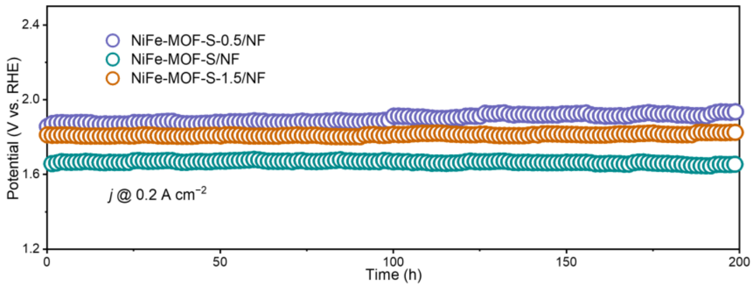

Fig. S37. OER durability test at a current density of 0.2 A cm^{-2} for NiFe-MOF-S-0.5/NF, NiFe-MOF-S/NF, and NiFe-MOF-S-1.5/NF in 1 M KOH + seawater.

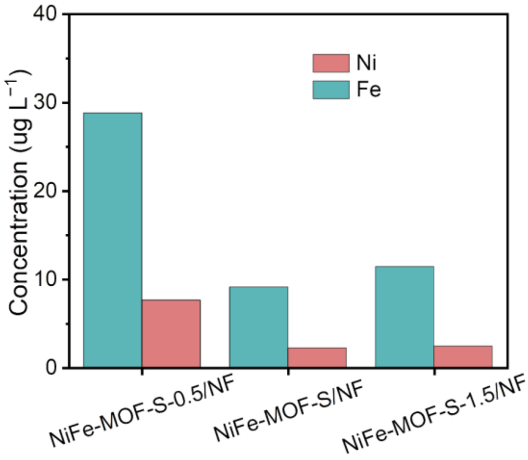

Fig. S38. The Ni and Fe concentrations leached in the electrolyte during OER for NiFe-MOF-S-0.5/NF, NiFe-MOF-S/NF, and NiFe-MOF-S-1.5/NF in 1 M KOH + seawater.

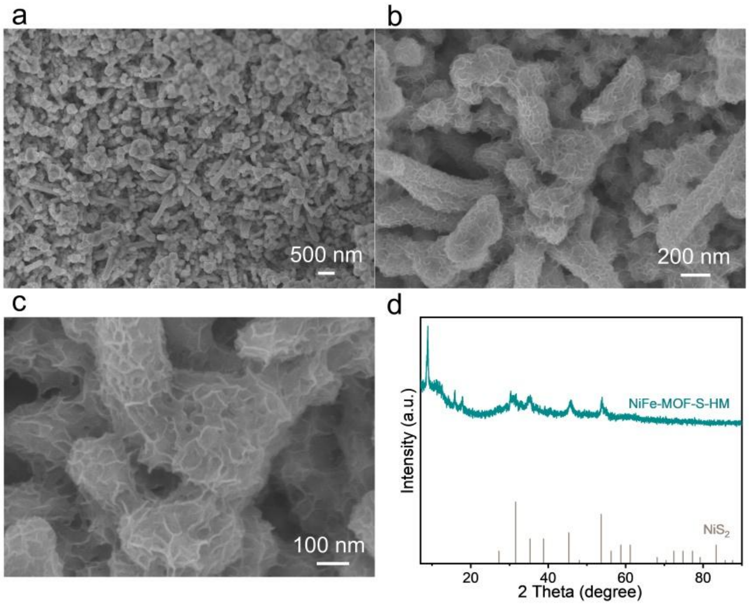

Fig. S39. SEM images of (a–c) NiFe-MOF-S-HM/NF. (d) XRD patterns of NiFe-MOF-S-HM detached from the NF substrate (NiS_2: PDF#11-0099).

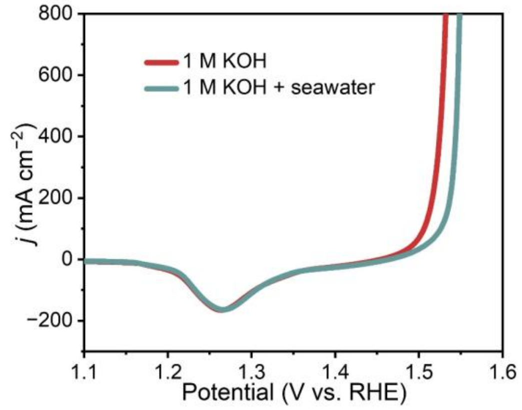

Fig. S40. LSV polarization curves for NiFe-MOF-S-HM/NF in 1 M KOH and 1 M KOH + seawater.

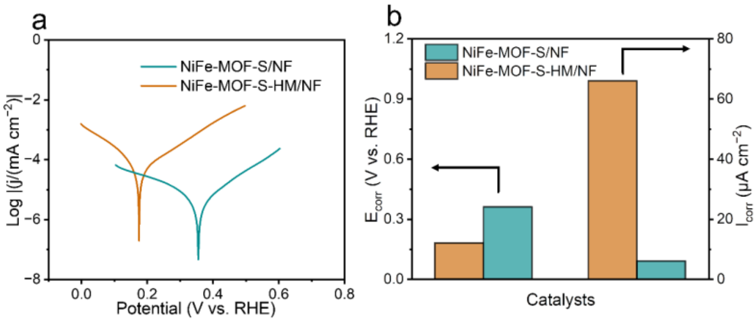

Fig. S41. (a) Tafel polarization curves of NiFe-MOF-S/NF and NiFe-MOF-S-HM/NF in 1 M KOH + seawater. (b) Comparison of E_{corr} and I_{corr} on NiFe-MOF-S/NF and NiFe-MOF-S-HM/NF in 1 M KOH + seawater.

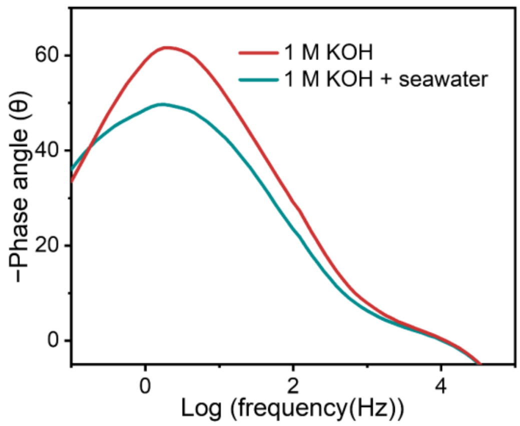

Fig. S42. Bode phase plots of NiFe-MOF-S/NF at 1.3 V vs. RHE in 1 M KOH and 1 M KOH + seawater.

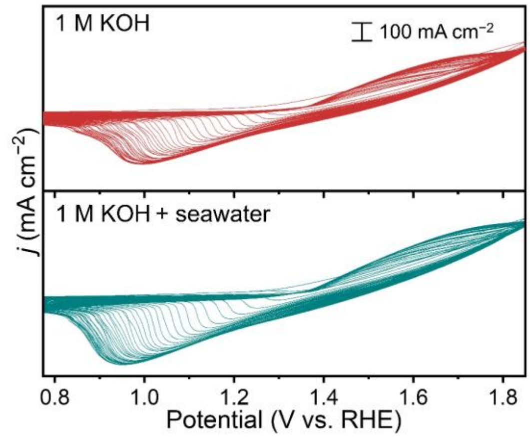

Fig. S43. The evolution of CV curves for NiFe-MOF-S/NF from the 1st to the 50th cycle in 1 M KOH and 1 M KOH + seawater at 20 mV s^{-1} between 0.774 and 1.85 V vs. RHE.

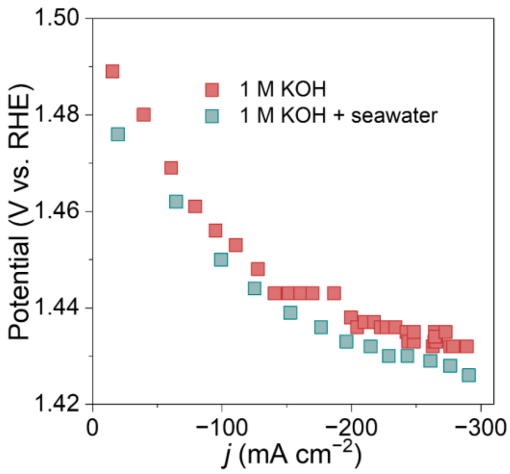

Fig. S44. Correlation between reduction peak current densities and the potential required to reach a current density of 100 mA cm^{-2} for NiFe-MOF-S/NF in alkaline water and alkaline seawater. The x-axis represents the reduction peak current densities extracted from the CV curves. The y-axis represents the potential required to reach a current density of 100 mA cm^{-2}.

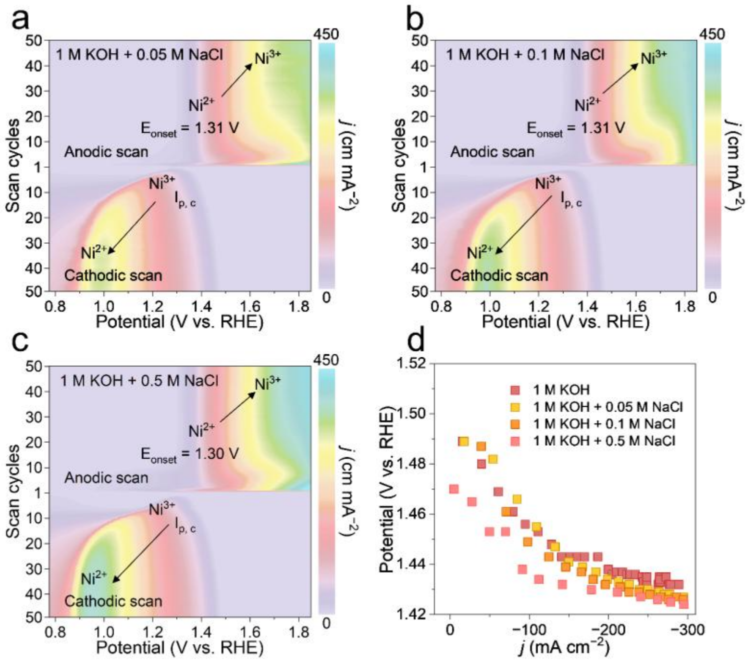

Fig. S45. (a, b, and c) The evolution of CV curves for NiFe-MOF-S/NF from the 1st to the 50th cycle in (a) 1 M KOH + 0.05 M NaCl, (b) 1 M KOH + 0.1 M NaCl, and (c) 1 M KOH + 0.5 M NaCl at 20 mV s^{-1} between 0.774 and 1.85 V vs. RHE. (d) Correlation between reduction peak current densities and the potential required to reach a current density of 100 mA cm^{-2} for NiFe-MOF-S/NF in 1 M KOH, 1 M KOH + 0.05 M NaCl, 1 M KOH + 0.1 M NaCl, and 1 M KOH + 0.5 M NaCl. The x-axis represents the reduction peak current densities extracted from the CV curves. The y-axis represents the potential required to reach a current density of 100 mA cm^{-2}.

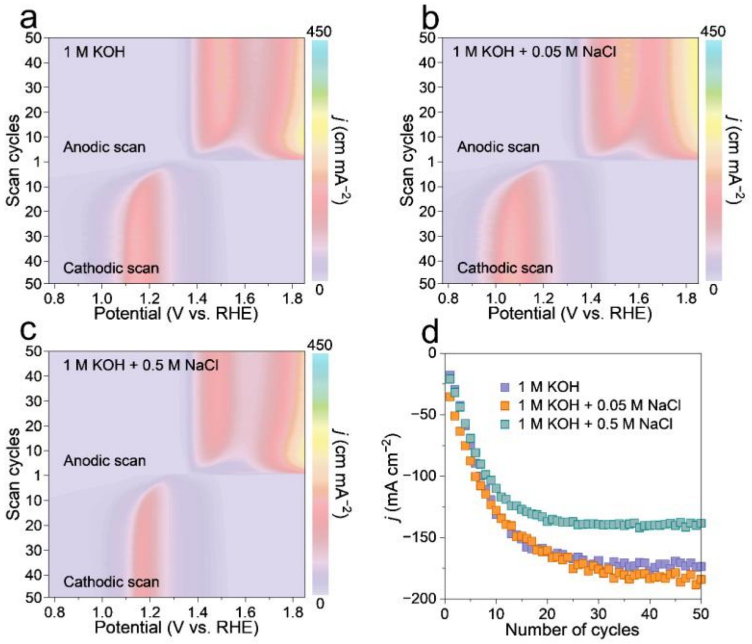

Fig. S46. (a, b, c) The evolution of CV curves for Ni-MOF/NF from the 1st to the 50th cycle in (a) 1 M KOH, (b) 1 M KOH + 0.05 M NaCl, and (c) 1 M KOH + 0.5 M NaCl at 20 mV s^{-1} between 0.774 and 1.85 V vs. RHE. (d) The variation of reduction peak current density with CV cycles for Ni-MOF/NF in 1 M KOH, 1 M KOH + 0.05 M NaCl, and 1 M KOH + 0.5 M NaCl.

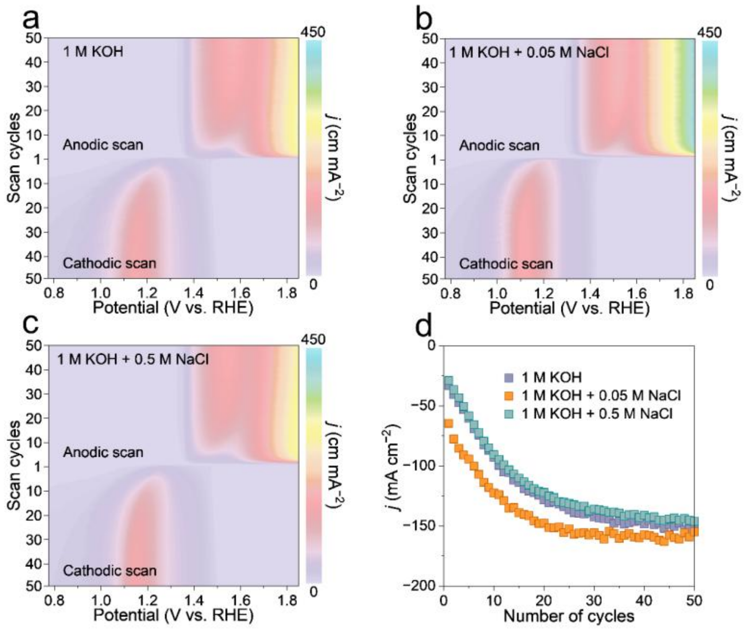

Fig. S47. (a, b, c) The evolution of CV curves for Fe-MOF/NF from the 1st to the 50th cycle in (a) 1 M KOH, (b) 1 M KOH + 0.05 M NaCl, and (c) 1 M KOH + 0.5 M NaCl at 20 mV s^{-1} between 0.774 and 1.85 V vs. RHE. (d) The variation of reduction peak current density with CV cycles for Fe-MOF/NF in 1 M KOH, 1 M KOH + 0.05 M NaCl, and 1 M KOH + 0.5 M NaCl.

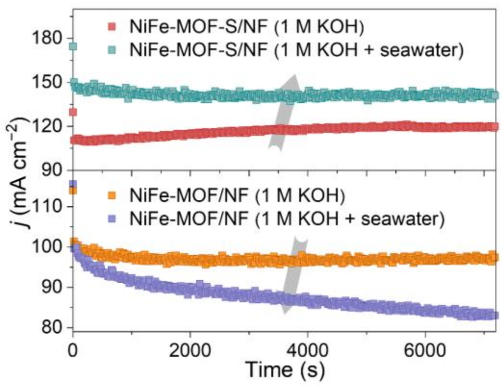

Fig. S48. Current–time (i–t) curves of NiFe-MOF/NF and NiFe-MOF-S/NF in 1 M KOH and 1 M KOH + seawater at 1.64 V vs. RHE.

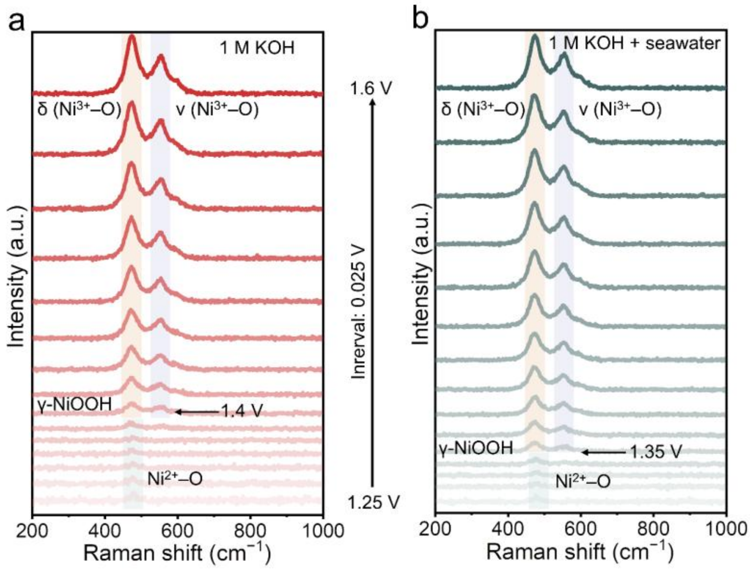

Fig. S49. Potential-dependent in-situ Raman spectra during the OER process in (a) 1 M KOH and (b) 1 M KOH + seawater.

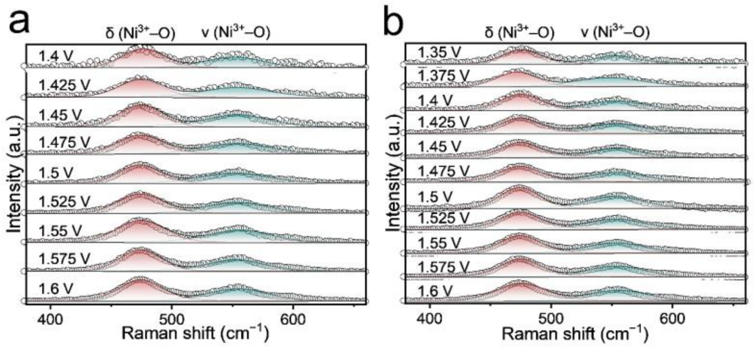

Fig. S50. In-situ Raman spectra of NiFe-MOF-S/NF versus potential in (a) 1 M KOH and (b) 1 M KOH + seawater. Two peaks at 475 and 555 cm^{-1} are corresponded to the bending and stretching vibrations of Ni^{3+}–O in NiOOH.

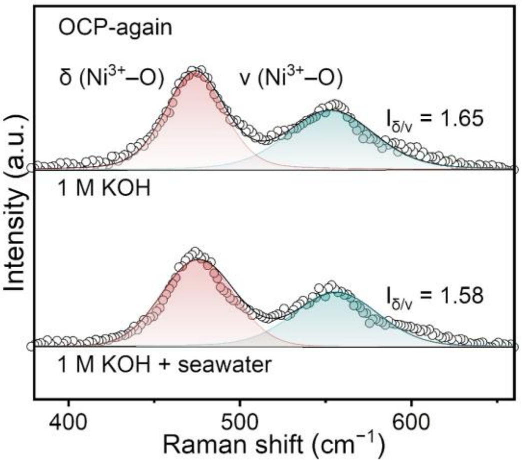

Fig. S51. The $I_{\delta/v}$ of NiFe-MOF-S/NF at OCP potential in 1 M KOH and 1 M KOH + seawater.

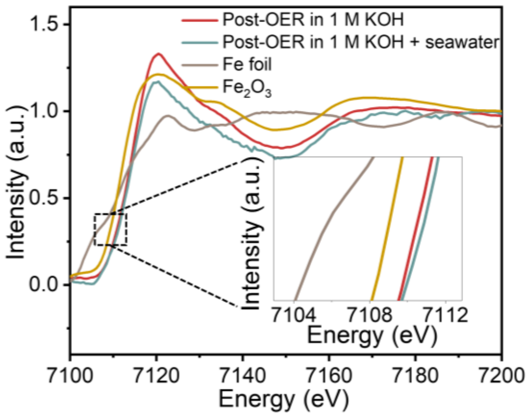

Fig. S52. Fe K-edge XANES spectra of Fe foil, Fe_2O_3, post-OER NiFe-MOF-S in 1 M KOH and 1 M KOH + seawater detached from the NF substrate (inset: expanded view of the absorption edge region).

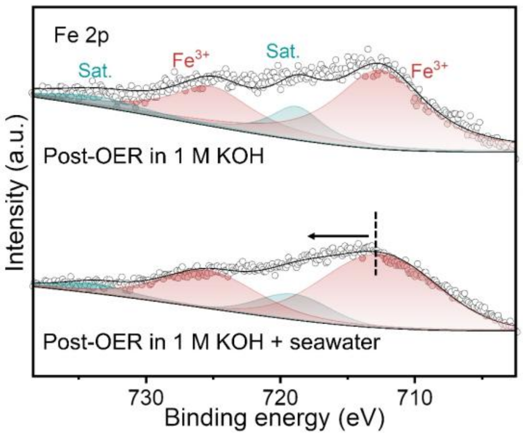

Fig. S53. XPS spectra of Fe 2p for post-OER NiFe-MOF-S detached from the NF substrate in 1 M KOH and 1 M KOH + seawater.

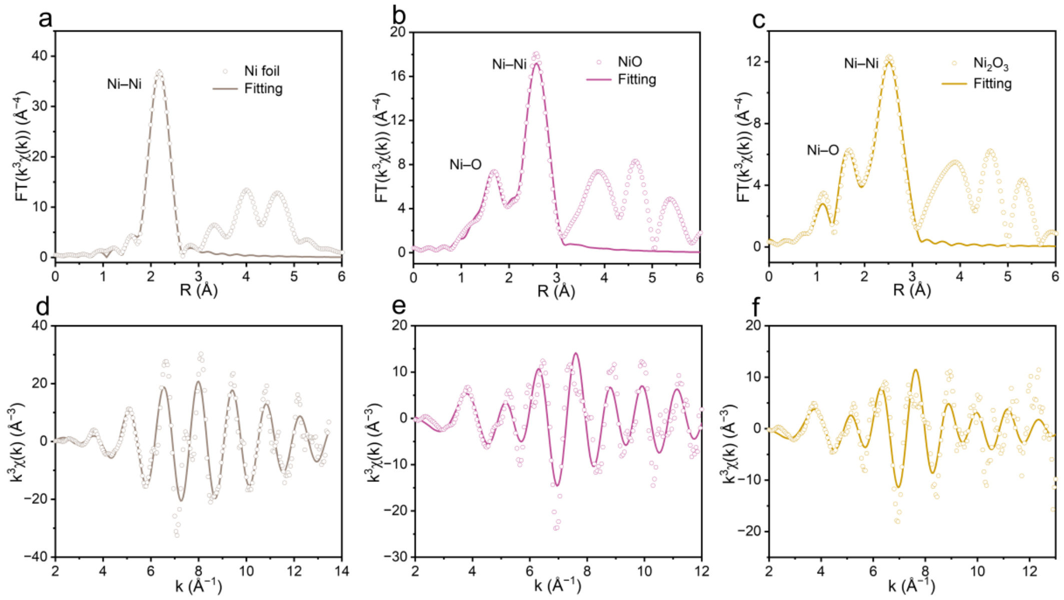

Fig. S54. The fitting analysis of k^3-weighted Fe K-edge EXAFS oscillations of Ni foil (a, d), NiO (b, e), and Ni_2O_3 (c, f) in k space (d, e, f) and FT to R space (a, b, c).

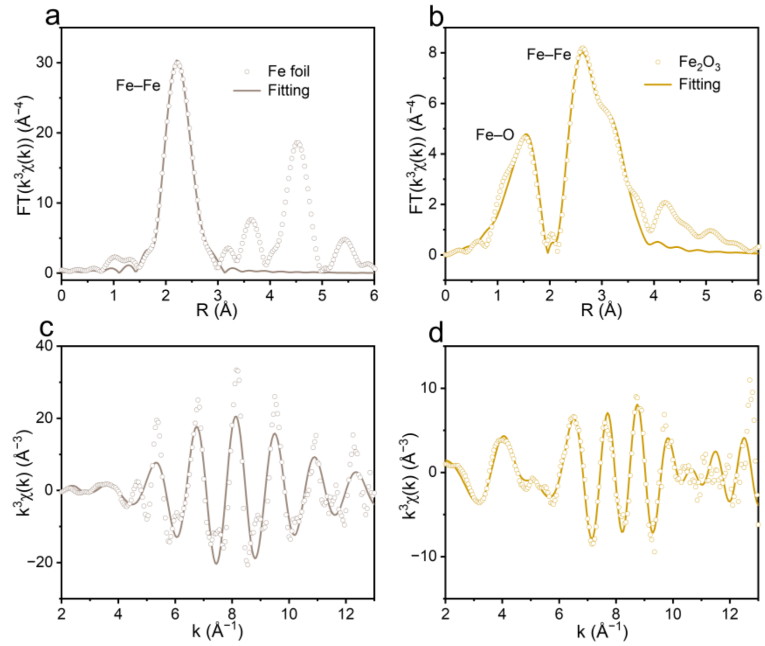

Fig. S55. The fitting analysis of k^3-weighted Fe K-edge EXAFS oscillations of Fe foil (a, c) and Fe_2O_3 (b, d) in k space (c, d) and FT to R space (a, b).

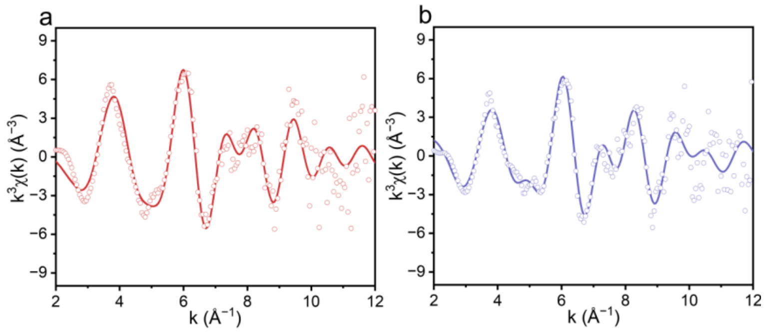

Fig. S56. The fitting curve of k^3-weighted EXAFS spectra of post-OER NiFe-MOF-S in 1 M KOH (a) and 1 M KOH + seawater (b).

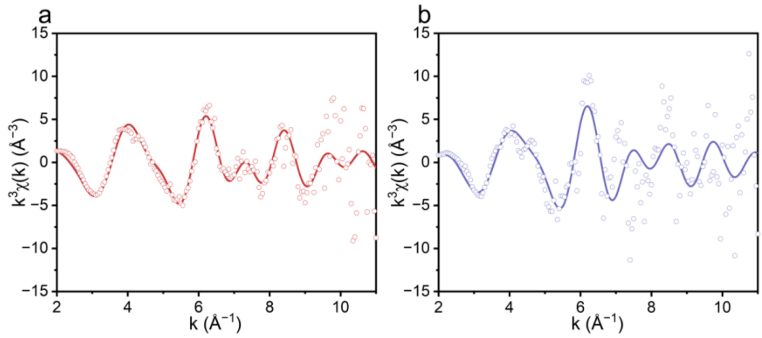

Fig. S57. The fitting curve of k^3-weighted EXAFS spectra of post-OER NiFe-MOF-S in 1 M KOH (a) and 1 M KOH + seawater (b).

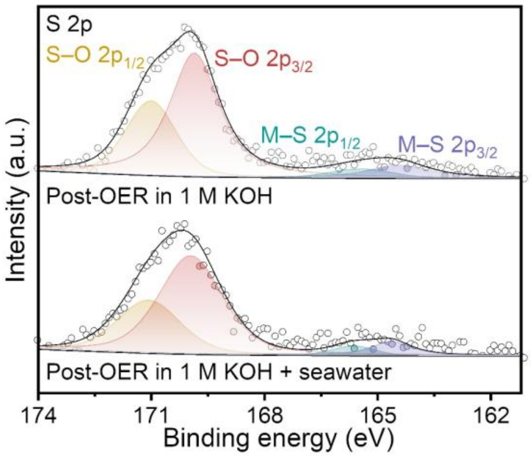

Fig. S58. XPS spectra of S 2p for the post-OER NiFe-MOF-S in 1 M KOH and 1 M KOH + seawater.

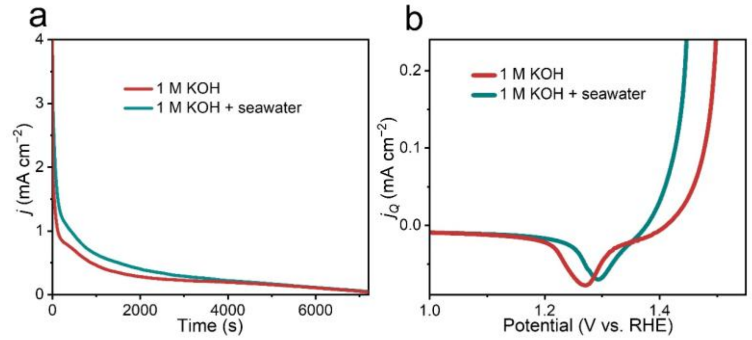

Fig. S59. (a) i–t curves of NiFe-MOF-S/NF in 1 M KOH and 1 M KOH + seawater at 1.23 V vs. RHE. (b) The normalized LSV polarization curves with the charge derived from the integration of i–t curves.

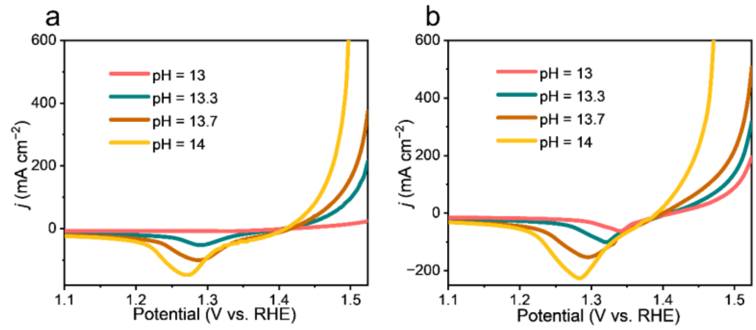

Fig. S60. The pH dependence of OER activity. The LSV polarization curves of NiFe-MOF-S/NF in (a) pure water and (b) seawater with different pH.

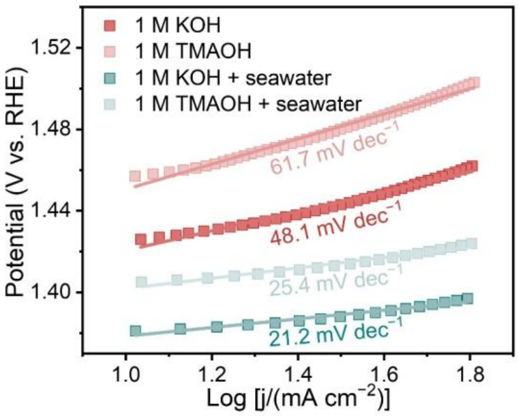

Fig. S61. The corresponding Tafel slopes for the LSV polarization curves of NiFe-MOF-S/NF in 1 M KOH, 1 M TMAOH, 1 M KOH + seawater, and 1 M TMAOH + seawater.

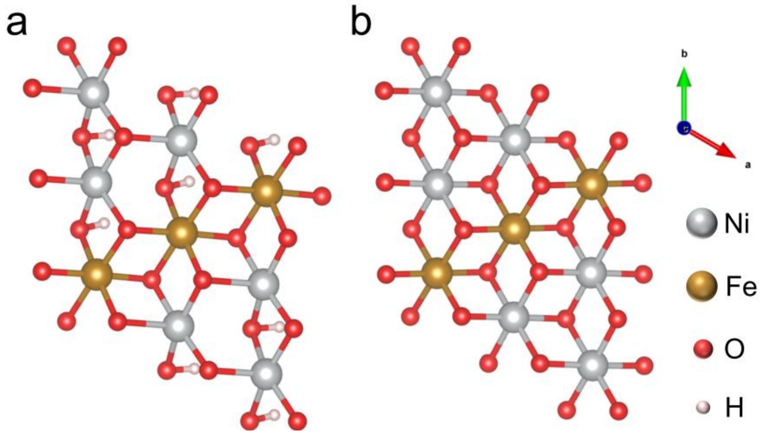

Fig. S62. Atomic structure models of (a) L-NiFeOOH and (b) S-NiFeOOH.

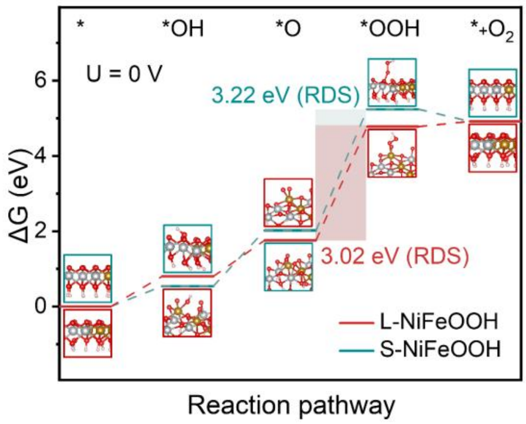

Fig. S63. The Gibbs free energy diagram of the OER process for the AEM on L-NiFeOOH and S-NiFeOOH at U = 0 V.

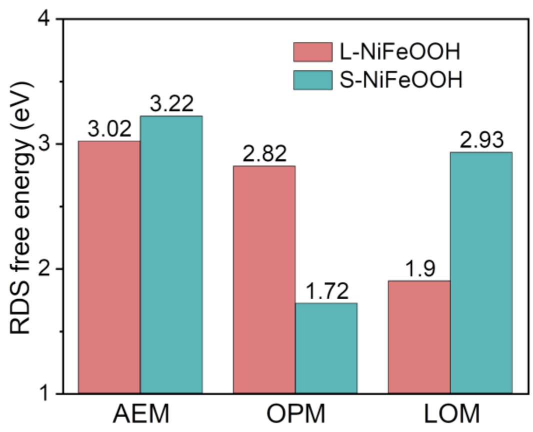

Fig. S64. Comparison of the ΔG in rate-determining step based on AEM, LOM, and OPM.

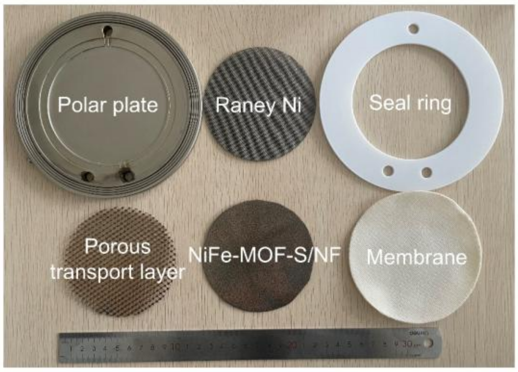

Fig. S65. Optical image for components included in a single cell.

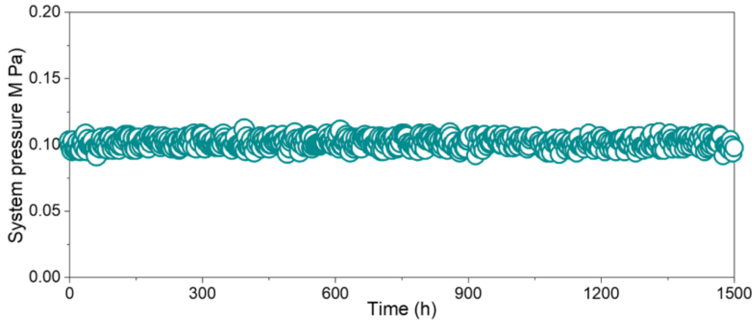

Fig. S66. System pressure of the 1.0 kW-scale ASWE for 1500-hour operation.

Fig. S67. Post-test photographs of the disassembled 1.0 kW ASWE showing the bipolar plate with three ports (electrolyte inlet/outlet, O_2 outlet, and H_2 outlet) after operation.

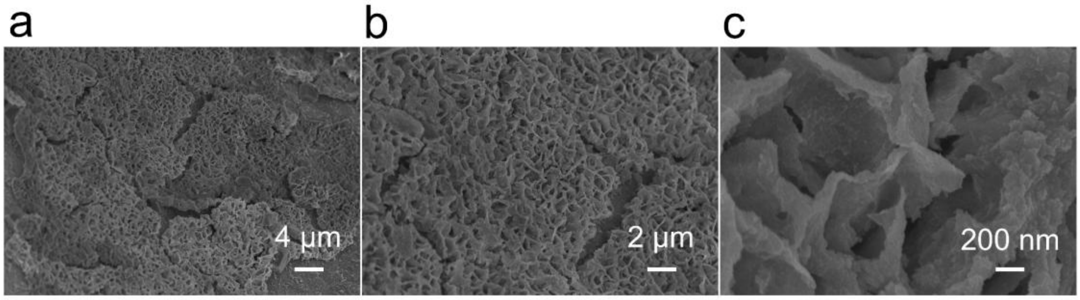

Fig. S68. SEM images of NiFe-MOF-S/NF after durability test in a 1.0 kW-scale ASWE.

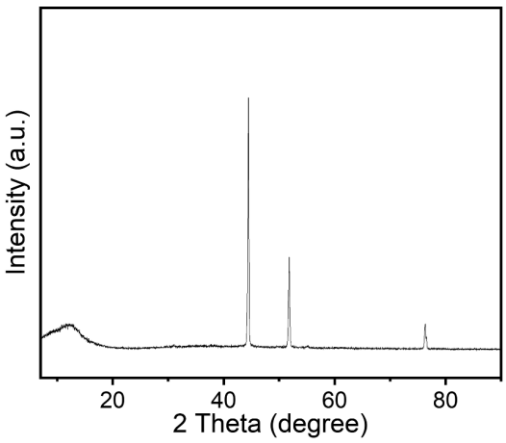

Fig. S69. XRD patterns of NiFe-MOF-S/NF after durability test in a 1.0 kW-scale ASWE.

Fig. S70. An optical image of the DEMS electrochemical cell.

Table S1. Comparison of the long-term durability and corresponding current density of NiFe-MOF-S/NF with recently reported state-of-the-art catalysts.

Catalysts	Electrolyte	Current density (mA cm^{-2})	Overpotential (mV)	Durability test	Reference
NiMoFe/NM	1 M KOH + seawater	10 100 500	253 332 440	550 h @ 100 mA cm^{-2}	*Adv. Energy Mater.* 2023, 14, 2303261.
CoFe-C_i@ GQDs/NF	Simulated seawater	100 500	254 320	2800 h @ 1200 mA cm^{-2}	*Nat. Sustain.* 2024, 7, 158–167.
TS-NiFe LDH/NF	1 M KOH + seawater	200 500 1000	296 344 412	350 h @ 1000 mA cm^{-2}	*Small* 2024, 20, 2311431.
Co_xP_v@NC	1 M KOH + seawater	500 1000	323 353	100 h @ 800 mA cm^{-2}	*Nano Energy* 2023, 109, 108292.
LDH-CeW@NFF	1 M KOH + seawater	500 1000	330 386.7	100 h @ 1000 mA cm^{-2}	*Appl. Catal. B-Environ.* 2023, 330, 122612.
60Fe/NF	1 M KOH + seawater	500	635	100 h @ 250 mA cm^{-2}	*Adv. Energy Mater.* 2023, 13, 2301921.
S-(Ni,Fe)OOH	1 M KOH + seawater	100 500 1000	300 398 462	100 h @ 100 mA cm^{-2}	*Energy Environ. Sci.* 2020, 13, 3439–3446.
Ni_2P-Fe_2P	1 M KOH + seawater	500	384	48 h @ 100 mA cm^{-2}	*Adv. Funct. Mater.* 2021, 31, 2006484.

Ag/NiFeRu LDH	1 M KOH + seawater	500	244	1000 h @ 1000 mA cm^{-2}	*Adv. Funct. Mater.* 2024, 34, 2315674.
Ni_3S_2/Fe-NiP_x /NF	1 M KOH + seawater	500 1000	336 351	225 h @ 50–180 mA cm^{-2}	*Adv. Sci.* 2022, 9, 2104846.
NiMoN/NiFeN	1 M KOH + seawater	100 500 1000	307 369 398	100 h @ 500 mA cm^{-2}	*Nat. Commun.* 2019, 10, 5106.
OP-NiCo-LDH	Simulated seawater	500	330	500 h @ 500 mA cm^{-2}	*Appl. Catal. B-Environ.* 2023, 332, 122749.
$Ni(MoS_x)_m(OH)_n$/MNF	1 M KOH + seawater	500	450	3000 h @ 500 mA cm^{-2}	*J. Energy Chem.* 2025, 107, 407–415.
Ag/NiFe LDH	1 M KOH + seawater	10 100 500 1000	217 246 279 303	1000 h @ 1000 mA cm^{-2}	*Nano Energy* 2022, 98, 107212.
RuMoNi	1 M KOH + seawater	100 500 1000	291 397 484	3000 h @ 500 mA cm^{-2}	*Nat. Commun.* 2023, 14, 3607.
NiFe-PPy	1 M KOH + seawater	10 100 500	250 302 371	2000 h @ 500 mA cm^{-2}	*Angew. Chem. Int. Ed.* 2024, 136, e202409628.
Os-Ni_4Mo/MoO_2	1 M KOH + seawater	500	336	2500 h @ 500 mA cm^{-2}	*Adv. Mater.* 2024, 36, 2408982.
CrO_4^{2-}-NiFe LDH/Cr_2O_3	1 M KOH + seawater	500	313	2500 h @ 1000 mA cm^{-2}	*Nat. Commun.* 2024, 15, 6624.

$Ni_3FeN@PO_4^{3-}/NF$	1 M KOH + seawater	500	329	2500 h @ 1000 mA cm^{-2}	*Adv. Mater.* 2025, 37, 2415421.
CAPist-S1	1 M KOH + seawater	500	193	4000 h @ 1000 mA cm^{-2}	*Adv. Sci.* 2025, 12, 2416661.
Fe-NiSOH	1 M KOH + seawater	10 100 500	213 263 311	900 h @ 500 mA cm^{-2}	*Energy Environ. Sci.* 2022, 15, 4647–4658.
NiFe LDH/NF (with KPF_6 as electrolyte additive)	1 M KOH + seawater + 20 mM PF_6^-	200 500	209 247	5000 h @ 1000 mA cm^{-2}	*Nat. Commun.* 2025, 16, 1–10.
Ir/NiOOH-Se@Cl	20 wt % NaOH + saturated NaCl	500	313	500 h @ 500 mA cm^{-2}	*J. Am. Chem. Soc.* 2025, 147, 20716–20724.
PW_{12}-CoFe LDH/NF	1 M KOH + seawater	500	325	1300 h @ 1000 mA cm^{-2}	*Nat. Commun.* 2025, 16, 5541.
ca-Mo-NiFePO/NMF	1 M KOH + seawater	500	328	1000 h @ 100 mA cm^{-2}	*Adv. Funct. Mater.* 2025, 2504862.
NiFe-LDH@Ag/IF	1 M KOH + seawater	500	286	1000 h @ 500 mA cm^{-2}	*Small* 2025, 21, 2503976.
B, Fe-CoP	1 M KOH + seawater	100 500 1000	282 349 376	100 h @ 200 mA cm^{-2}	*Adv. Funct. Mater.* 2024, 34, 2402264.
$Fe\text{-}Ni_2P_v$	1 M KOH + seawater	100 500 1000	180 270 306	110 h @ 100 mA cm^{-2}	*Adv. Mater.* 2024, 36, 2307395.

$(NiFe)C_2O_4$/NF	1 M KOH + seawater	100 500	280 339	600 h @ 1000 mA cm^{-2}	*Angew. Chem. Int. Ed.* 2024, 63, e202316522.
NiS@LDH	1 M KOH + seawater	10 100 500 1000	242 279 311 341	100 h @ 200 mA cm^{-2}	*Small* 2023, 19, 2300194.
NiCoP foam	1 M KOH + seawater	10 500 1000	391 327 356	300 h @ 1000 mA cm^{-2}	*J. Mater. Chem. A* 2024, 12, 2680−2684.
$P_{4.8}$-NiFe ANs-400	1 M KOH + seawater	500 1000	293 325	100 h @ 250 mA cm^{-2}	*Appl. Catal. B-Environ.* 2024, 342, 123376.
MnCo/NiSe	1 M KOH + seawater	10 500	261.3 419.4	200 h @ 500 mA cm^{-2}	*Appl. Catal. B-Environ.* 2023, 325, 122355.
CeNiFe@CuO	1 M KOH + seawater	500	280	300 h @ 500 mA cm^{-2}	*Adv. Funct. Mater.* 2025, 2508539.
NiMo	1 M KOH + seawater	500	288	1000 h @ 500 mA cm^{-2}	*Adv. Funct. Mater.* 2025, 2509590.
F-NiFe-LDH	1 M KOH + seawater	500	375	1000 h @ 1000 mA cm^{-2}	*Adv. Funct. Mater.* 2025, 35, 2423965.
3DOM-HEH-300	1 M KOH + seawater	500	278	400 h @ 100 mA cm^{-2}	*Adv. Mater.* 2025, e06068.
NiFe-LDH/$NiMoO_4$	1 M KOH + seawater	500	339	100 h @ 1000 mA cm^{-2}	*Adv. Funct. Mater.* 2025, 2417603.

$(NiCoMnCrFe)_3O_4$	1 M KOH + seawater	500	384	170 h @ 500 mA cm^{-2}	SusMat. 2025, 5, e70010.
HS-$Fe_{0.17}Co_{0.83}Se_2$	1 M KOH + seawater	500	322	250 h @ 1000 mA cm^{-2}	*Adv. Funct. Mater.* 2025, 35, 2419626.
$NiCoP_v$@NF	1 M KOH + seawater	500	414	50 h @ 100 mA cm^{-2}	*Adv. Energy Mater.* 2024, 14, 2400975.
$Ni_{0.10}$-Fe_3N@NCPs	1 M KOH + seawater	500	312	200 h @ 500 mA cm^{-2}	*Adv. Funct. Mater.* 2024, 34, 2404470.
Nb-NiOOH-O_v	1 M KOH + seawater	500	345	170 h @ 100 mA cm^{-2}	*ACS Nano* 2025, 19, 9070–9080.
(Ni,Fe)OOH@Ni_xP	1 M KOH + seawater	100 500	262 318	100 h @ 500 mA cm^{-2}	*Appl. Catal. B-Environ.* 2023, 336, 122926.
NiFeO-CeO_2/NF	1 M KOH + seawater	500 1000	338 408	200 h @ 1000 mA cm^{-2}	*ACS Nano* 2023, 17, 16008–16019.
CoFe-Ni_2P	1 M KOH + seawater	10 100 500	224 274 360	500 h @ 500 mA cm^{-2}	*Adv. Energy Mater.* 2023, 13, 2301475.
Cr-Co_XP	1 M KOH + seawater	100 500 1000	334 392 423	140 h @ 100 mA cm^{-2}	*Adv. Funct. Mater.* 2023, 33, 2214081.
NF/Ni-MnO_2@FePA	1 M KOH + seawater	500	330	125 h @ 500 mA cm^{-2}	*ACS Catalysis.* 2025, 15, 6954–6968.

$Fe_2P/Ni_{1.5}Co_{1.5}N/N_2P$	1 M KOH + seawater	50 100 500	240 255 307	40 h @ 100 mA cm^{-2}	*ACS Nano* 2023, 17, 1681–1692.
F-FeCoPv@IF	1 M KOH + seawater	100 500 1000	290 330 370	20 h @ 100 mA cm^{-2}	*Appl. Catal. B-Environ.* 2023, 328, 122487.
Ni_xCr_yO	1 M KOH + seawater	100 500	370 460	2250 h @ 10 mA cm^{-2}	*Angew. Chem. Int. Ed.* 2023, 62, e202309854.
$Fe(Cr)OOH/Fe_3O_4$	1 M KOH + seawater	10 100 500	219 251 278	100 h @ 100 mA cm^{-2}	*Appl. Catal. B-Environ.* 2022, 302, 120847.
$Au\text{-}Gd\text{-}Co_2B@TiO_2$	1 M KOH + seawater	100 500	280 330	200 h @ 500 mA cm^{-2}	*Appl. Catal. B-Environ.* 2022, 301, 120836.
$CoP_x@FeOOH$	1 M KOH + seawater	100 500	283 337	80 h @ 500 mA cm^{-2}	*Appl. Catal. B-Environ.* 2021, 294, 120256.
NiCoS/NF	1 M KOH + seawater	500	440	100 h @ 100 mA cm^{-2}	*Appl. Catal. B-Environ.* 2021, 291, 120071.
NiFe-MOF-S/NF	1 M KOH + seawater	10 100 500	151 174 213	7000 h @ 1000 mA cm^{-2}	This work

Table S2. EXAFS data fitting results of samples.

<table>
<tr><th>Sample</th><th>Path</th><th>CN^a</th><th>R(Å)^b</th><th>σ^2 (Å^2)^c</th><th>ΔE_0(eV)^d</th><th>R factor</th></tr>
<tr><td colspan="7">Ni K-edge (S_0^2=0.795)</td></tr>
<tr><td>Ni foil</td><td>Ni–Ni</td><td>12.0*</td><td>2.48</td><td>0.0061</td><td>6.0</td><td>0.0039</td></tr>
<tr><td rowspan="2">NiO</td><td>Ni–O</td><td>6.0</td><td>2.09</td><td>0.0059</td><td rowspan="2">−1.8</td><td rowspan="2">0.0063</td></tr>
<tr><td>Ni–Ni</td><td>12.0</td><td>2.96</td><td>0.0071</td></tr>
<tr><td rowspan="2">Ni_2O_3</td><td>Ni–O</td><td>6.0</td><td>2.09</td><td>0.0050</td><td rowspan="2">−3.4</td><td rowspan="2">0.0092</td></tr>
<tr><td>Ni–Ni</td><td>12.0</td><td>2.95</td><td>0.0076</td></tr>
<tr><td rowspan="2">NiFe-MOF-S</td><td>Ni–O</td><td>6.0</td><td>2.06</td><td>0.0093</td><td rowspan="2">−3.8</td><td rowspan="2">0.0188</td></tr>
<tr><td>Ni–S</td><td>6.0</td><td>2.39</td><td>0.0121</td></tr>
<tr><td rowspan="3">post-OER NiFe-MOF-S in 1 M KOH</td><td>Ni–O</td><td>5.8</td><td>2.05</td><td rowspan="2">0.0143</td><td rowspan="2">−12.5</td><td rowspan="3">0.0341</td></tr>
<tr><td>Ni–S</td><td>5.0</td><td>2.24</td></tr>
<tr><td>Ni–M</td><td>4.0</td><td>3.13</td><td>0.0095</td><td>2.1</td></tr>
<tr><td rowspan="3">post-OER NiFe-MOF-S in 1 M KOH + seawater</td><td>Ni–O</td><td>5.3</td><td>1.97</td><td>0.0032</td><td rowspan="3">3.2</td><td rowspan="3">0.0129</td></tr>
<tr><td>Ni–S</td><td>4.0</td><td>2.16</td><td>0.0083</td></tr>
<tr><td>Ni–M</td><td>5.1</td><td>2.93</td><td>0.0105</td></tr>
<tr><td colspan="7">Fe K-edge (S_0^2=0.813)</td></tr>
<tr><td rowspan="2">Fe foil</td><td>Fe–Fe</td><td>8.0*</td><td>2.49</td><td>0.0055</td><td rowspan="2">8.5</td><td rowspan="2">0.0056</td></tr>
<tr><td>Fe–Fe</td><td>6.0*</td><td>2.86</td><td>0.0087</td></tr>
<tr><td rowspan="4">Fe_2O_3</td><td>Fe–O</td><td>5.9</td><td>1.99</td><td>0.0112</td><td rowspan="4">−2.0</td><td rowspan="4">0.0132</td></tr>
<tr><td>Fe–Fe</td><td>3.3</td><td>2.96</td><td rowspan="3">0.0036</td></tr>
<tr><td>Fe–Fe</td><td>2.4</td><td>3.38</td></tr>
<tr><td>Fe–Fe</td><td>3.2</td><td>3.69</td></tr>
<tr><td rowspan="2">NiFe-MOF-S</td><td>Fe–O</td><td>6.0</td><td>1.98</td><td>0.0102</td><td rowspan="2">−9.2</td><td rowspan="2">0.0131</td></tr>
<tr><td>Fe–S</td><td>6.0</td><td>2.17</td><td>0.0291</td></tr>
<tr><td rowspan="3">post-OER NiFe-MOF-S in 1 M KOH</td><td>Fe–O</td><td>5.9</td><td>1.96</td><td>0.0153</td><td>−13.8</td><td>0.0294</td></tr>
<tr><td>Fe–S</td><td>4.5</td><td>2.16</td><td>0.0153</td><td>−13.8</td><td rowspan="2">0.0294</td></tr>
<tr><td>Fe–M</td><td>3.0</td><td>3.15</td><td>0.0066</td><td>9.4</td></tr>
<tr><td rowspan="3">post-OER NiFe-MOF-S in 1 M KOH + seawater</td><td>Fe–O</td><td>5.7</td><td>2.03</td><td rowspan="2">0.0055</td><td rowspan="2">5.4</td><td rowspan="3">0.0077</td></tr>
<tr><td>Fe–S</td><td>4.0</td><td>2.27</td></tr>
<tr><td>Fe–M</td><td>4.8</td><td>2.96</td><td>0.0106</td><td>−11.7</td></tr>
</table>

^{a}*CN*, coordination number; ^{b}*R*, the distance between absorber and backscatter atoms; $^c\sigma^2$, the Debye-Waller factor value; $^d\Delta E_0$, inner potential correction to account for the difference in the inner potential between the sample and the reference compound; *R* factor indicates the goodness of the fit. S_0^2 was fixed to 0.795 and 0.813, according to the experimental EXAFS fit of Ni foil and Fe foil by fixing *CN* as the known crystallographic value. *This value was fixed during EXAFS fitting based on the known structure of Ni and Fe. Fitting conditions: *k* range: 2.0–10.0; *R* range: 1.0–3.5 (NiFe-MOF-S, post-OER

NiFe-MOF-S in 1 M KOH, and post-OER NiFe-MOF-S in 1 M KOH + seawater); 2.0–11.0; *R* range: 1.0–3.5; fitting space: R space; *k*-weight = 3. A reasonable range of EXAFS fitting parameters: $0.800 < S_0^2 < 1.000$; $CN > 0$; $\sigma^2 > 0$ Å^2; $|\Delta E_0| < 15$ eV; *R* factor < 0.02.

Table S3. The characteristic FTIR peak positions of different oxygen containing intermediate species reported in previous literature.

Bond type	Wavelength number (cm^{-1})	Reference
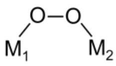	1078	*Energy Environ. Sci.* 2020, 13, 2200–2208.
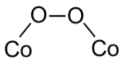	1014	*Chem.* 2021, 7, 2101–2117.
Metal–O–O	1124	*J. Electrochem. Soc.* 2002, 149, A1293.
Ce–O–O	1126	*J. Am. Chem. Soc.* 1989, 111, 7683–7687.
Li–O–O	1127	*J. Phys. Chem. C* 2017, 121, 19657–19667.
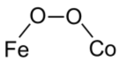	1160–1170	*Proc. Natl. Acad. Sci. USA* 2024, 121, e2317247121.
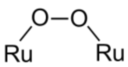 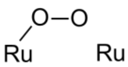	1089, 1128	*Nat. Catal.* 2021, 4, 1012–1023.
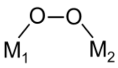 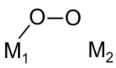	1122, 1136	*J. Am. Chem. Soc.* 2023, 145, 7829–7836.
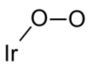	1126	*Nat. Commun.* 2024, 15, 95.